A bond model for DEM simulation of cementitious materials and deformable structures

Brown, N. J., Chen, J. F., & Ooi, J. Y. (2014). A bond model for DEM simulation of cementitious materials and deformable structures. *Granular Matter*, *16*(3), 299-311. https://doi.org/10.1007/s10035-014-0494-4

Published in:
Granular Matter

Document Version:
Peer reviewed version

A bond model for DEM simulation of cementitious materials and deformable structures

Nicholas J Brown

Institute for Infrastructure and Environment, School of Engineering, The University of Edinburgh, The King's Buildings, Edinburgh EH9 3JL, Scotland, U.K.

Jian-Fei Chen

School of Planning, Architecture and Civil Engineering, Queen's University Belfast, David Keir Building, Belfast, BT9 5AG, Northern Ireland, U.K.

Jin Y Ooi

Institute for Infrastructure and Environment, School of Engineering, The University of Edinburgh, The King's Buildings, Edinburgh EH9 3JL, Scotland, U.K.

Corresponding author:

j.ooi@ed.ac.uk

Abstract

There is an increasing use of the discrete element method (DEM) to study cemented (e.g. concrete and rocks) and sintered particulate materials. The chief advantage of the DEM over continuum based techniques is that it does not make assumptions about how cracking and fragmentation initiate and propagate, since the DEM system is naturally discontinuous. The ability for the DEM to produce a realistic representation of a cemented granular material depends largely on the implementation of an inter-particle bonded contact model. This paper presents a new bonded contact model based on the Timoshenko beam theory which considers axial, shear and bending behaviour of the bond. The bond model was first verified by simulating both the bending and dynamic response of a simply supported beam. The loading response of a concrete cylinder was then investigated and compared with the Eurocode equation prediction. The results show significant potential for the new model to produce satisfactory predictions for cementitious materials. A unique feature of this model is that it can also be used to accurately represent many deformable structures such as frames and shells, so that both particles and structures or deformable boundaries can be described in the same DEM framework.

Keywords: Discrete Element Method (DEM), Bond Model, Cementitious Materials, Numerical Modelling

Introduction

A number of numerical techniques have been used to study the behaviour of cementitious materials such as rock and concrete. The focus of these techniques is often placed on determining the strength and failure characteristics. For many of these techniques cementitious materials are treated as homogeneous continua, but they are naturally inhomogeneous at the microscopic scale. This means that continuous models often only describe the material behaviour in an average sense [1]. The Discrete Element Method (DEM), first proposed by Cundall [2] for the study of rock mechanics and later expanded for modelling granular materials [3], is ideally suited for studying cementitious materials due to their naturally discrete inhomogeneous structure. The DEM uses the repeated execution of three steps, namely contact detection, calculation of interaction forces and numerical time integration to solve the interaction of a collection of particles.

The objective of this study is to investigate the failure of cementitious materials through bond breakage mechanics at the particle scale. The focus is placed on whether realistic bulk properties, including the strength and macroscopic failure mode can be reproduced. The failure of cementitious materials is highly influenced by the initiation and propagation of cracks that occur at cemented grain interfaces. The ability of the DEM to produce a realistic representation of a cementitious material depends largely on the assumption that bonds exist between particles resisting their separation. The behaviour of individual bonds is governed by the contact laws contained within bond models. These laws can be seen as the formulation of the material model at the microscopic level [4] and are probably the most important part of the model [1]. It is the behaviour at the contacts which influences the overall mechanical behaviour. One of the main concerns when using the DEM is to ensure that the appropriate contact laws and microscopic parameters are used to represent the subject material at the macroscopic scale [5].

A number of different bonded contact models have been developed. The simplest of these is probably the spring model such as [6] which connects the centres of interacting particles. They are capable of resisting the relative displacement of bonded particles in compression and tension; there is no resistance against shear, bending or twisting actions. An improved bonded contact model was developed by Potyondy and Cundall [7] where particles are connected by a point of glue which is represented by a pair of elastic springs with a constant normal and shear stiffness [8]. This was further developed by the authors into the more complex parallel bond model [7] which has since been used by many researchers [e.g. 8,9]. The bonded contacts in the parallel bond model can be considered as "a set of elastic springs uniformly distributed over the cross section with a constant normal and shear bond stiffness lying on the contact plane and centred at the contact point" [8]. In addition to normal and shear forces, the parallel bond is also able to transmit moments.

In some instances, especially where polygonal elements are used the bond between elements can be considered as a series of springs across the interface between two elements. This bonded contact type has been borrowed from the finite element method; a detailed description of this bond type is provided by D'Addetta et al [10].

Another bond representation is the use of beam elements, which are assumed to link the centres of particles in a bonded contact e.g. [11-14]. The contact laws can be based on Euler-Bernoulli or Timoshenko beam theory, and the elements are able to resist tensile force and bending and twisting moments. Schneider et al. [11] highlighted that beam models provide a good compromise between computational time and accuracy. The use of beam elements to represent cementitious materials may also be found in regular [15, 16] or random [17] lattice models. However, particle based models, unlike lattice models, permit frictional contacts to exist between particles after beam failure has occurred.

A variety of work has been conducted using bonded particle models to study the behaviour of cementitious materials under different loading conditions. Most of the work has covered the behaviour of cementitious materials under quasi-static

uni-axial loading, such as rock in 2D [8] and 3D [6, 7], and concrete in 2D [18] and 3D [12]. A uni-axial loading test is often used to calibrate models for different materials. The influence of strain rate on behaviour and dynamic loading has also been investigated [19-21], including the impact of missiles on concrete beams studied in 2D [22]. Sawamoto [23] used a bonded particle model to examine the dynamic impact of deformable missiles on reinforced concrete. Rock cutting, involving the interaction between a cutting element and a rock material, has also been studied in 3D [4, 9].

There are many derivations for the constitutive relationships contained within inter-particle bonded contact models, but from fundamental mechanics either a strut (spring) model or a beam model may be used. A strut model only resists the axial force, but is simple to implement and fast for computation; beam models are more computationally expensive but provide more realistic representations of the bond mechanism as they can take into account axial, bending, shear and torsion behaviour at a cemented joint [11, 13, 14].

In this paper a new bonded contact model is presented; the bond behaviour is based on the Timoshenko beam theory which is suited to describing the behaviour of short beams [24]. The model is used to study both cemented granular materials and deformable structures. In the following sections, the bonded contact model is first presented. It is verified by comparing the predictions with the beam bending theory, and then used to simulate an unconfined uni-axial compression test of a concrete cylinder sample. The manner in which the developed model uses breakable beams to connect an assembly of DEM particles is similar to those employed by other authors [e.g. 12, 25].

The Timoshenko Beam Bond Model (TBBM)

A cementitious material may be represented by an assembly of DEM particles. For simplicity, spherical particles are used in this study. These particles may interact at either bonded or non-bonded contacts; only one contact can exist between any two particles due to their spherical nature. At a non-bonded contact a spring-dashpot configuration is assumed with the constitutive behaviour being

described using the Hertz-Mindlin contact law [26, 27]. At a bonded contact a virtual bond element is considered to exist between the particles joining them together. Each bond element is assumed to be circular and straight in three dimensional space at formation. Both contact types resist compressive and shear forces, but bonded contacts can also resist tensile forces as well as bending and twisting moments. Material damage may be represented directly through the breakage of bonds, although more complex damage models can be included. This enables the response of the subject material to load to be studied as damage develops in the system.

At each bonded contact a Timoshenko beam element is assumed to rigidly connect the two particles in contact. The behaviour of this bond is assumed to follow the Timoshenko beam theory [24]. For simplicity, it is assumed that the beam element connects to the centres of the two particles (Fig.1) so that each end of the bond shares the same six degrees of freedom as the particle. Note that there are no difficulties to implement if it is desirable to assume that the bond element connects the two adjacent particles away from their respective centres.

In Fig. 1 the two ends of a single bond, marked as points α and β, are shown to connect to the centres of particles A and B respectively; the bond has a length L_b and a radius r_b. Vectors $\{P_A\}$ and $\{P_B\}$ define the positions of the two particles in the global Cartesian co-ordinate system (X, Y, Z).

$$\{P_i\} = \{X_i \quad Y_i \quad Z_i\} \quad i = A, B \tag{1}$$

In addition to the single global co-ordinate system each bond has its own unique local co-ordinate system (x, y, z), as shown in Fig. 1, with the x axis originating at α and passing through β. The length of this bond is therefore:

$$L_b = \|P_B - P_A\| = x_\beta - x_\alpha \tag{2}$$

where x_α and x_β are the x-coordinates of the two ends of the beam in the local coordinate system.

The bonds are assumed to have no mass in the DEM model – all mass is appropriately assigned to the particles. They are subjected to internal forces caused by relative displacements and rotations of the particles they connect.

The Timoshenko beam theory, which is suited for stocky beams for which the shear deformation is important, can be used to relate the internal forces and moments to the particle displacements and rotations. In this study, the internal forces are calculated in an incremental manner. In each time step, the increment of the internal forces (and moments) are determined from the incremental displacements (and rotations) at the bond ends (particles) using the Timoshenko beam theory:

$$\{\Delta F\} = [K] \cdot \{\Delta u\} \tag{3}$$

where the incremental force vector $\{\Delta F\}$ and displacement (rotation) vector $\{\Delta u\}$ are

$$\{\Delta F\} = \{\Delta F_{\alpha x} \;\; \Delta F_{\alpha y} \;\; \Delta F_{\alpha z} \;\; \Delta M_{\alpha x} \;\; \Delta M_{\alpha y} \;\; \Delta M_{\alpha z} \;\; \Delta F_{\beta x} \;\; \Delta F_{\beta y} \;\; \Delta F_{\beta z} \;\; \Delta M_{\beta x} \;\; \Delta M_{\beta y} \;\; \Delta M_{\beta z}\}^T \tag{4}$$

$$\{\Delta u\} = \{\Delta d_{\alpha x} \;\; \Delta d_{\alpha y} \;\; \Delta d_{\alpha z} \;\; \Delta \theta_{\alpha x} \;\; \Delta \theta_{\alpha y} \;\; \Delta \theta_{\alpha z} \;\; \Delta d_{\beta x} \;\; \Delta d_{\beta y} \;\; \Delta d_{\beta z} \;\; \Delta \theta_{\beta x} \;\; \Delta \theta_{\beta y} \;\; \Delta \theta_{\beta z}\}^T \tag{5}$$

in which $\{\Delta F\}$ contains 12 force (F) and moment (M) increments at the two ends of the bond, $\{\Delta u\}$ contains 12 displacement (d) and rotation (θ) increments at the two ends of the bond, and [K] is a 12×12 tangential stiffness matrix. The location and positive direction of both the rotations and moments follow the right hand rule. The internal total forces (F) and moments (M) are shown in Fig. 2. Each force (moment) and displacement (rotation) has two subscripts: α or β denoting the two ends of the bond, and x, y or z denoting the direction of the force in the local coordinate system of the bond (e.g. $\Delta F_{\alpha x}$ is the force increment in x direction at the α end).

For small deformation linear elastic bonds, the tangential stiffness matrix [K] remains constant before failure, and its general form can be derived from the differential equations for beam deformation using the unit displacement theory for a Timoshenko beam, as presented by Przemieniecki [24]:

$$[K] = \begin{bmatrix} K_1 & -K_2 & -K_1 & -K_2 \\ K_2 & K_3 & -K_2 & K_4 \\ -K_1 & K_2 & K_1 & K_2 \\ K_2 & K_4 & -K_2 & K_3 \end{bmatrix} \tag{6}$$

where

$$[K_1]=\begin{bmatrix} \frac{E_b A_b}{L_b} & 0 & 0 \\ 0 & \frac{12k}{L_b{}^2(1+\Phi)} & 0 \\ 0 & 0 & \frac{12k}{L_b{}^2(1+\Phi)} \end{bmatrix} \quad (7)$$

$$[K_2]=\begin{bmatrix} 0 & 0 & 0 \\ 0 & 0 & \frac{-6k}{L_b(1+\Phi)} \\ 0 & \frac{6k}{L_b(1+\Phi)} & 0 \end{bmatrix} \quad (8)$$

$$[K_3]=\begin{bmatrix} \frac{k}{(1+v_b)} & 0 & 0 \\ 0 & \frac{k(4+\Phi)}{(1+\Phi)} & 0 \\ 0 & 0 & \frac{k(4+\Phi)}{(1+\Phi)} \end{bmatrix} \quad (9)$$

$$[K_4]=\begin{bmatrix} \frac{-k}{(1+v_b)} & 0 & 0 \\ 0 & \frac{k(2-\Phi)}{(1+\Phi)} & 0 \\ 0 & 0 & \frac{k(2-\Phi)}{(1+\Phi)} \end{bmatrix} \quad (10)$$

in which:

$$k=\frac{E_b I_b}{L_b} \quad (11)$$

where E_b is the Young's modulus, v_b the Poisson's ratio, A_b the cross sectional area and I_b the second moment of area of the bond, and Φ the Timoshenko shear coefficient, where:

$$A_b=r_b^2\pi \quad (12)$$

$$I_b=\frac{r_b^4\pi}{4} \quad (13)$$

$$\Phi = \frac{f_s 12 E_b I_b}{G_b A_b {L_b}^2} = \frac{20 {r_b}^2 (1+\nu_b)}{3 {L_b}^2} \quad (14)$$

where G_b is the bond's shear modulus and f_s is the form factor for shear, which for a circular cross section can be estimated to be 10/9 [29].

The displacement increment of a particle between two consecutive iterations can be determined from the standard DEM calculation cycle [3]. In the present study for each bonded contact the displacement increment of the two particles in the global coordinate system is stored as a vector $\{u_g\}$. The displacement increment of the bond ends in the local co-ordinate system is determined by multiplying the global displacement increment vector by the transformation matrix $[\gamma]$, so that:

$$\{u\} = \begin{bmatrix} \gamma & & & \\ & \gamma & & \\ & & \gamma & \\ & & & \gamma \end{bmatrix} \{u_g\} \qquad (15)$$

The transformation matrix $[\gamma]$ contains nine directional cosines, which represent the nine angles between the three vectors defining the axes of the global co-ordinate system ({X} {Y} {Z}) and the three vectors defining the axes of the local co-ordinate system ({x} {y} {z}).

$$[\gamma] = \begin{bmatrix} x_X & x_Y & x_Z \\ y_X & y_Y & y_Z \\ z_X & z_Y & z_Z \end{bmatrix} \quad (16)$$

Each element in the transformation matrix contains a letter which represents the local coordinate axis and a subscript which represents the global coordinate axis. For example the directional cosine x_Y defines the cosine of the angle between the vectors defining the local x axis and the global Y axis. The transformation matrix thus consists of three vectors that define the local co-ordinate system:

$$\{\hat{x}\} = \{x_X \quad x_Y \quad x_Z\}^T \qquad (17)$$

$$\{\hat{y}\} = \{y_X \quad y_Y \quad y_Z\}^T \qquad (18)$$

$$\{\hat{z}\} = \{z_X \quad z_Y \quad z_Z\}^T \qquad (19)$$

As shown in Fig.1 the local *x* axis follows the longitudinal axis of the beam bond, so that:

$$\{\hat{x}\} = \frac{P_B - P_A}{L_b} \qquad (20)$$

The *y* axis is calculated first using the cross product of the local *x* axis vector, and the global *Z* axis vector $\hat{Z}$. The angle between *x* and *y* axes is 90°. The normalised *y* axis can be determined as:

$$\{\hat{y}\} = \frac{\hat{Z} \times \hat{x}}{\left|\hat{Z}\right| \left|\hat{x}\right|} \qquad (21)$$

This shall always produce a local *y* axis, unless the vectors *Z* and *x* are collinear in which case:

$$\{\hat{y}\} = \{0 \quad 1 \quad 0\}^T \qquad (22)$$

The local *z* axis can then be determined as the cross product of the local *x* axis vector and the local *y* axis vector, such that:

$$\{\hat{z}\} = \frac{\hat{x} \times \hat{y}}{\left|\hat{x}\right| \left|\hat{y}\right|} \qquad (23)$$

Assuming small deformation, the total internal forces and moments at the bond ends at any time can be determined by summing increments from the start of the simulation:

$$\{F\} = \sum \Delta F \qquad (24)$$

where $\{F\}$ contains 12 total forces and moments.

$$\{F\} = \{F_{\alpha x} \quad F_{\alpha y} \quad F_{\alpha z} \quad M_{\alpha x} \quad M_{\alpha y} \quad M_{\alpha z} \quad F_{\beta x} \quad F_{\beta y} \quad F_{\beta z} \quad M_{\beta x} \quad M_{\beta y} \quad M_{\beta z}\}^T \qquad (25)$$

In this study the bonds are assumed to behave in a linear elastic and brittle manner (more sophisticated models will be considered in future research); a bond fails if one of the maximum stresses exceeds the corresponding strength. Three strength criteria are considered: compressive, tensile and shear. The maximum compressive stress σ_{Cmax}, tensile stress σ_{Tmax} and shear stress τ_{max} in each bond are determined from beam theory such that:

$$\sigma_{Ci} = \left(\frac{F_{\beta x}}{A_b} - \frac{r_b \sqrt{M_{iy}^2 + M_{iz}^2}}{I_b} \right) \quad i = \alpha, \beta \tag{26}$$

$$\sigma_{C\max} = -\min\left(\sigma_{C\alpha}, \sigma_{C\beta}\right) \tag{27}$$

$$\sigma_{Ti} = \left(\frac{F_{\beta x}}{A_b} + \frac{r_b \sqrt{M_{iy}^2 + M_{iz}^2}}{I_b} \right) \quad i = \alpha, \beta \tag{28}$$

$$\sigma_{T\max} = \max\left(\sigma_{T\alpha}, \sigma_{T\beta}\right) \tag{29}$$

$$\tau_{\max} = \frac{|M_{\alpha x}| r_b}{2I_b} + \frac{4\sqrt{F_{\alpha y}{}^2 + F_{\alpha z}{}^2}}{3A_b} \tag{30}$$

If at any iteration a bond does not fail then a set of forces equal but opposite to the total bond end forces (moments) $\{F\}$ are applied to the respective particles. If a bond fails the bonded contact is removed and cannot be reintroduced.

At a non-bonded contact (either non-bonded from the beginning or arisen from broken bonds) where there is a physical interaction between a particle and either a boundary geometry or another particle, the Hertz-Mindlin contact law is used to determine the contact forces. The Hertz-Mindlin contact model has been used extensively in the DEM modelling of granular materials [e.g. 30-32].

Implementation of the Timoshenko Beam Bond Model

For the purposes of this study the Timoshenko Beam Bond Model has been implemented in the three-dimensional discrete element software EDEM [33]

through an Application Programming Interface. The software EDEM has a number of useful features which allow easy implementation and efficient computation. One such feature is the capability to store custom properties for particles and contacts; utilising this capability, the stiffness matrix and failure criteria for each bond are determined immediately after the bond initialisation procedure and stored as custom contact properties. The bonded contact model requires a small number of bond parameters to be defined by the user. These include the Young's modulus E_b, the Poisson's ratio ν_b, and the mean and coefficient of variation for the compressive, tensile and shear strengths.

The incremental bond end displacements are determined by multiplying the time-step by the velocities of the particles the bond connects to. These calculations are the same as those used for particle motion in EDEM [3]. The model assumes that the increments of the bond end rotations over a single computational time step are small; this does not present a problem in this study as the bonded structure is very stiff so the displacements and rotations of particles within a small time-step are indeed very small. The incremental displacements and rotations found in simulations presented in this paper are of the order of $\times 10^{-5}$ mm and $\times 10^{-6}$ rad respectively.

Bond initialisation

Part of the material model preparation process is the bond initialisation procedure which is conducted after an assembly of particles has been generated. During the bond initialisation procedure particles will be bonded together if their contact radii overlap. A particles contact radius is calculated by multiplying its physical radius by a user-defined contact radius multiplier η. If the value of η is increased above unity, bonds are formed between particles which are not necessarily in direct contact, this is a similar formulation to models [e.g. 34-36] but different to others [e.g. 6] where physical particle overlap is required for a bond to form.

At the end of the bond initialisation procedure an initial stress free state is achieved by resetting all physical overlaps to zero. This state is attained by storing, as a custom contact property, any physical overlap that exists between

two elements during the bond initialisation procedure. This "initial" overlap is then subtracted from each subsequent determination of overlap at each contact, resulting in a static assembly of bonded particles with zero overlap and no contact force at the start of each loading simulation. Resetting the overlaps is an important process as otherwise when bonds are broken the contact overlaps may produce exaggerated contact forces leading to non-physical behaviour. However, it is important to note that an initial stress free state is not always desired, e.g. in excavation or tunnelling at depth where the rock is subject to an in-situ stress, it would be very easy to remove the resetting of overlaps routine from the model if required. After the bonds have been inserted between particles initialisation of bonds the cementitious material model is completed and ready for testing.

The literature reports many different ways in which the bond radius can be determined, for example either using the arithmetic or harmonic means of the two particles' radii [5]. In the implementation presented here, if a bond is considered to connect particles *A* and *B* (as shown in Fig. 1), the radius of that bond is assumed to be:

$$r_b = \lambda \cdot \min(r_A, r_B) \qquad (31)$$

where r_A and r_B are the radii of particles *A* and *B* respectively and the numerical parameter λ is a bond radius multiplier. By including the bond radius multiplier flexibility is introduced into the way the bond radius is determined. For all simulations presented in this paper a bond radius multiplier of one was used. As the bond is assumed to be prismatic its radius is assumed to be that matching the smallest particle as this will be the weakest point when determining stresses in the bond.

Bond strength characterization

The model in this study incorporates a stochastic variation of the bond strength. The compressive σ_C, tensile σ_T and shear τ strength of the bonds in the model are each assumed to follow a Gaussian distribution defined by a mean and a coefficient of variation, so that:

$$\sigma_C = S_C \cdot ((\varsigma_C \cdot N) + 1) \qquad (32)$$

$$\sigma_T = S_T \cdot \left(\left(\varsigma_T \cdot N \right) + 1 \right) \qquad (33)$$

$$\tau = S_S \cdot \left(\left(\varsigma_S \cdot N \right) + 1 \right) \qquad (34)$$

where S_C, S_T and S_S are respectively the mean compressive, tensile and shear strength of the bonds; ς_C, ς_T, ς_S are, respectively, their coefficient of variation; N is a random number from a standard normal distribution. The random value of N is assigned to each bond and applied equally to each of the three strength calculations (Eqs 32-34). The bond strengths are limited to within a range of between zero and twice the mean strength.

Model verification

Verifying the implementation of a numerical model is an important step to ensure that the mathematical descriptions in the programmed code match the theory underpinning the model. In order to verify the TBBM, a series of benchmark tests have been conducted, including those verifying the behaviour of a single bond oriented in different directions and under tensile, compressive, shear, twisting and bending loading actions. As an extension of this process further tests involved the construction of simple structural elements which are subjected to different loading actions. Only the static and dynamic loading responses for a simply supported beam are summarised below, which demonstrate that the bond model behaves as a Timoshenko beam.

Static loading of a simply supported beam

A simply supported beam can be formed by bonding a number of particles in a line; an example with five particles is shown in Fig. 3. The extreme left-hand particle is fixed against all translational displacement, the extreme right hand particle is fixed against vertical translational displacements, and both particles can rotate freely in plane. All out-of-plane displacements are prevented.

All of the bonds forming the beam have the same material and geometrical properties throughout, so the spacing or the number of particles should not affect its response. For a circular beam under a mid-span point load W, the theoretical mid-span deflection δ is:

$$\delta = \frac{WL^3}{48EI} + \frac{WLf_s}{4GA} \qquad (35)$$

where L is the length, EI is the flexural rigidity and GA/f_s is the shear rigidity of the beam. In the DEM simulation the bonds representing the sections of the beam are given material properties for steel so that E_b = 200 GPa and ν_b = 0.3. The radius of the bonds is r_b = 0.1 m and the form factor for shear f_s for a circular cross section is 10/9. Bonds are initialised so that a beam of total length L = 6 m is formed. In the simulation a central load of 100 kN is applied to the particle at the centre of the beam and the predicted transverse deflection recorded. For beams made of between three and 31 particles the predicted mid span deflections are shown in Table 1. These are compared with a theoretical mid-span deflection of 28.7169 mm determined using Eqn. 35 showing a very good agreement between theory and DEM simulation irrespective of the number of bonds used to form the simply supported beam.

Free vibration of a simply supported beam

The dynamics of the model are verified using the three particle DEM representation of the above simply supported beam (Fig. 3) subjected to free vibration. As the bonds are massless, the only mass affecting the beam vibration is from the concentrated mass of the central particle.

The fundamental natural frequency $f_{natural}$ for this beam is [37]:

$$f_{natural} = \frac{1}{2\pi}\sqrt{\frac{K_{beam}}{m}} \qquad (36)$$

where m is the mid-span mass and K_{beam} is the beam's stiffness given by:

$$K_{beam} = \frac{192EIGA}{4L^3GA + 48f_sEIL} \qquad (37)$$

If the central particle has a mass of 1000 kg then the theoretical fundamental natural frequency for this beam is found from Eqn. 36 to be 9.392 Hz.

In the DEM simulation, the central particle is displaced 10 mm vertically and then set free to vibrate as shown in Fig. 4. The DEM predicted fundamental natural frequency is 9.407 Hz which is only 0.16% greater than the theoretical solution.

Application to cementitious materials

The capabilities of the new model are examined in the simulation of a cementitious material under uni-axial compression loading. In this instance the material being represented is concrete. To this end the predictive capabilities of the model are tested against four macroscopic properties that characterise the quantitative response of the material, these are: the ultimate strength f_c', the strain at ultimate strength ε_c, the secant bulk modulus $E_{c(0.4)}$ (determined at 40% of the ultimate strength) and the bulk Poisson's ratio $\nu_{c(0.4)}$ (again determined at 40% of the ultimate strength). In addition to these bulk properties, the failure mechanism is also of key interest.

This study explores the plausibility that the developed model can be used to reproduce the important bulk (macroscopic) characteristics of concrete for engineering applications when particles and bonds represent the structure of the subject material at the mesoscopic scale. Particles and bonds do not directly represent individual grains and cement interfaces but rather represent the constituent parts of the subject material and their interactive properties at the mesoscopic scale. In the material model concrete is represented by a dense assembly of bonded polydisperse spherical particles with all the mass of the system represented by these particles.

Initial particle assembly and bond network

It is very important when conducting any DEM modelling that the particle packing generated is representative of the problem that is to be solved. Good assemblies for concrete should not include preferable crack paths [13] with macroscopic isotropy being obtained. Initial computational trials using the model highlighted the importance of generating a dense network of particles and bonds to improve the predictive capabilities of the model for cementitious materials. One way to achieve this is to ensure a particle packing with a very high solid fraction. This is advantageous over using a more porous structure compensated with a higher contact radius multiplier, as a high solid fraction ensures that there is

sufficient load carrying capacity through both bonded and non-bonded contacts (activated after bonded contacts break) which has been found to produce a more realistic loading stiffness and post peak behaviour.

Initial tests showed that particle assemblies with high solid fractions couldn't be easily obtained with the generation techniques available in the EDEM software; the dynamic techniques used (gravitational deposition and compaction) led to unwanted anisotropy at the macroscopic scale and were computationally expensive, the constructive technique used (a sequential inhibition model) could not produce a low enough porosity with the co-ordination numbers always being lower than desired. Instead a collective rearrangement technique using the software GiD [38] and developed by Labra et al. [39] was used to produce a cylindrical specimen of 100 mm diameter and 200 mm height; the cylinder specimen (shown in Fig. 5) consists of 28,982 spherical particles. Particle polydispersity was introduced to avoid crystalline formation; a uniform particle size distribution was imposed with the minimum particle radius r_{min} = 1.15 mm and the maximum particle radius r_{max} = 2.71 mm. Using this generation technique a dense particle packing with a measured bulk porosity of 0.37 was achieved. This porosity is simply a property that relates to the tightness of the particle packing achieved by the collective rearrangement technique it does not directly relate to the porosity of the subject material (which for concrete would be expected to be much lower).

For the simulations presented in this paper the contact radius multiplier η was set at 1.1. This value was chosen through modelling trials which proved that this value was suitable for providing a sufficient bond network to mimic a realistic stress-strain response. Using this contact radius multiplier, a total of 119,109 bonds were generated; meaning initially that there was an average of 8.22 bonds per particle; the distribution of bond coordination number is shown in Fig. 6. When the particle generation and bond initialisation procedures were completed the final concrete model was ready for the loading simulation to begin. As at the end of the bond initialisation procedure all particle-particle and particle-geometry overlaps were set to zero, and no gravity was considered in the loading

simulation, the material model had no internal or external forces acting upon it when the uni-axial loading simulation began.

Model input parameters

The developed model uses a relatively large number of input parameters. However through an extensive parametric study the relative importance of these parameters has been determined. The number of parameters that need to be determined can be reduced by providing appropriate values for parameters that have minimal influence on the bulk response. This ultimately leads to a solution with the same predictive power but fewer input parameters.

Since the primary interest of this study is to produce a DEM model that can predict the ultimate strength and loading response of concrete, a calibration procedure can be used to determine a relationship between the key model parameters and the predicted bulk response. In the example presented in this paper a range of bulk behaviour was achieved by only varying the Young's modulus, the mean tensile strength and the mean shear strength of the bonds. The remaining input parameters were kept constant and are summarised in Table 2. To further simplify the model the shear strength is set to be equal to the tensile strength.

When simulating the uni-axial compression of the concrete cylinder, the numerical specimen was loaded by moving both top and bottom platens against each other to give a total strain rate of 1 s^{-1}. This rather high strain rate has significant computational advantage and was investigated separately to ensure stability. It was found that when using a strain rate of 1 s^{-1} the predicted bulk response did not significantly differ to that when the strain rate was two orders of magnitude lower. However, strain rates of an order of magnitude higher were seen to produce a significantly different stress-strain response. The computational time-step Δt was modified in line with the stiffness of the system to ensure a stable explicit integration. The time step was determined as a fraction of the critical time step, which is the largest time step for which a force is not transmitted beyond the nearest neighbours of a particle. As both bonded and non-bonded contacts are considered, the critical computational time step is determined for both, Δt_{bcrit} and

Δt_{HMcrit} respectively, with the lower of these two values being used to determine the computational time-step:

$$\Delta t = \xi \min\left(\Delta t_{bcrit}, \Delta t_{HMcrit}\right) \qquad (38)$$

where ξ is a factor that should be kept in the range of zero to one, with values of 0.1 to 0.2 being recommended [40]. For non-bonded contacts, the critical time step is determined using the Rayleigh time step, which is the time taken for a shear wave to propagate though a solid particle [26], for each particle the critical time step is determined as:

$$\Delta t_{HMcrit} = \frac{\pi r_p \left(\frac{\rho_p}{G_p}\right)^{0.5}}{\left(0.1631 v_p + 0.8766\right)} \qquad (39)$$

As the particle density ρ_p, shear modulus G_p and Poisson's ratio v_p are constant for all particles in the assembly the critical non-bonded time step is that for the smallest particle radius. The critical time step for bonded contacts is estimated from an approximate solution based on a single degree of freedom in a mass spring system [40]:

$$t_{bcrit} = 2\sqrt{\frac{m_{p\min}}{K_{b\max}}} \qquad (40)$$

The critical time step is determined for each bonded contact using the smallest particle mass $m_{p\min}$ and the largest bond stiffness component $K_{b\max}$ for that contact. For the simulation ξ was selected to be 0.05 and the time step calculated to be 1×10^{-7} s. For this study, the combination of loading rate and time step was chosen to ensure minimal dynamic effects with a total of 10,000 calculation steps required to be computed for the specimen to displace 1 mm; as a result, the dynamic effects were minimal [8].

At non-bonded contacts, energy is usually dissipated through frictional sliding and the spring-dashpot contact in the model. This was not deemed sufficient to arrive at a quasi-static solution in the computation steps employed. An additional non-viscous damping was applied to the whole system by damping the equations of motion as described in [41]; a damping coefficient of 0.5 was used in this study. For this simulation the total computational time was approximately 4 hours on a quad-core desktop PC.

Predicted behaviour of concrete under uniaxial compression

A calibration procedure was conducted with the target to produce a concrete specimen with an ultimate strength of 48 MPa and a realistic loading response [42]. For this, the required bond Young's modulus E_b was found to be 40 GPa and the mean bond tensile strength S_T was found to be 105 MPa. The stress-strain response and the corresponding bond breakage are shown in Fig. 7.

The stress-strain curve shown in Fig.7 indicates a close to linear but gradually softening ascending branch with a loss of stiffness noted after approximately $\varepsilon = 0.0008$ (43% of the strength) when 5% of the bonds have failed. This is consistent with physical experiments on concrete where under loading up to about 30% to 40% of the ultimate compressive strength, there is little additional micro-cracking observed between the aggregates and hardened cement paste (bond cracks); and the stress-strain response is close to, but not quite, linear elastic [43, 44]. The loss of stiffness increased with a rise in the number of broken bonds until the peak stress was reached. This loss of stiffness was caused by the continual failure of bonds resulting in a reduction in the overall stiffness of the bond network.

Bond breakage was initiated from very early on during loading because a relatively high coefficient of variation of strength for both tensile and shear was used to represent the stochastic variation of the bond strengths. This resulted in the weaker bonds failing at low loading levels which is reflected in the macroscopic loss of bulk stiffness. The rate of bond failure increased as the loading continued towards the peak failure and after the peak stress, the rate began to decrease in the softening regime. Figure 8 shows the failure modes of these broken bonds. It is noted that although the concrete is under compression, the overwhelming failure mode is through tension with a small proportion failing in shear and a negligible number failing in compression. This is consistent with the findings of other authors including [7].

The overall failure mechanism of the cylindrical specimen under uni-axial compression can be discerned from Fig. 9 which shows a cross sectional slice of the specimen in the post peak regime, at an axial strain of 0.0027. It shows that

the axial compression has led to an inclined rupture plane closely associated with the plane of maximum shear stress, and from the bond failure information, this shear cracking zone comprised overwhelmingly with bonds failing under tension.

As well as using the quantitative measures of the bulk behaviour, the overall stress-strain response and post-peak behaviour were also considered. A comparison between the DEM predicted stress-strain relationship and an empirical relationship can be made. Many compressive stress-strain relationships have been proposed for concrete [see 45], including the following Eurocode 2 [46] equation:

$$\frac{\sigma}{f_c'} = \frac{1.05\frac{E_{c(0.4)}}{E_f}\frac{\varepsilon}{\varepsilon_c} - \left(\frac{\varepsilon}{\varepsilon_c}\right)^2}{1 + \left(1.05\frac{E_{c(0.4)}}{E_f} - 2\right)\left(\frac{\varepsilon}{\varepsilon_c}\right)} \qquad (41)$$

where E_f is the secant modulus of elasticity at failure:

$$E_f = \frac{f_c'}{\varepsilon_c} \qquad (42)$$

The Eurocode EN 1992-1-1:2004 also provides an empirical relationship between the ultimate strength f_c' of a concrete cylinder and both the bulk secant modulus $E_{c\,(0.4)}$ and the strain at ultimate strength ε_c (see Table 3 in [46]):

$$E_{c(0.4)} = 22\sqrt[3]{(f_c'/10)} \qquad (43)$$

$$\varepsilon_c = 0.0007\left(f_c'\right)^{0.31} \le 0.0028 \qquad (44)$$

The Eurocode curve for any target strength case can therefore be determined by substituting Eqs 42, and 43 into 41.

In addition to the case presented above two further target strength cases (28 MPa and 68 MPa) were assessed and the behaviour of all three cases compared against the Eurocode prediction. These additional target strength cases provided simulations for two typical concrete strength classes reflected in the Eurocode. In order to obtain the input parameters for these additional cases the same calibration procedure as before was used. The values adopted for the model parameters for all three cases are shown in Tables 2 and 3.

The DEM produced stress-strain responses for the three cases are compared to the predictions made using the Eurocode relationship in Fig. 10. The progression of the number of broken bonds is shown in Fig. 11. The DEM predicted bulk properties are compared to the target properties from the Eurocode (derived from Eqs 43 and 44) in Table 4.

It can be seen from Table 4 that in all three cases, the models predicted the ultimate strength and the ultimate strain within 1.6% of the target values calculated using the Eurocode equation. However, the bulk stiffness is significantly underestimated, though this underestimation is reduced as the ultimate strength increases. The predicted bulk Poisson's ratio remained constant at 0.19 for all three cases, which is an appropriate value for concrete. Timoshenko and Gere [29] suggested that the Poisson's ratio for concrete should fall in the range of 0.1 to 0.2; Mehta and Monterio [44] and Neville and Brooks [47] suggested a slightly narrower range of 0.15 to 0.20 when determined from strain measurements.

Also, the model generally predicts a more brittle post peak response than that given by the Eurocode (Fig.10). The primary failure mode for all three cases is through the failure of bonds under tension, forming a shear crack zone. Figure 11

shows that when normalized the initial breakage of bonds is very similar for all three specimens but the eventual number of broken bonds reduces as the target strength increases.

It is suggested that for a given particle packing arrangement, the model can accurately predict the ultimate strength and strain at failure. However, the model under predicts the initial stiffness when compared to the Eurocode equation. Although the bonds could be stiffened to create a stiffer initial bulk response additional plasticity would be required for the strain at failure to match the Eurocode prediction. To enhance the model's capabilities some non-linearities could be added to the bond behaviour for improved modelling of the ductility of concrete. Examples of including non-linear stiffness terms can be found in the literature, e.g. [6] and [11]. Alternatively bond breakage could be encouraged through a reduction of the shear or compressive strengths. An investigation in to the suitability of these methods for achieving greater softening behaviour is beyond the scope of this paper.

Potential applications to deformable structures

In addition to the application of the developed model for studying the behaviour of concrete under uni-axial compression, there are many other potential applications. The theoretical solutions to the loading of simple structural elements are known and well understood. As the bond is based on beam theory, the model is capable of analyzing conventional structural elements such as beams, frames, plates and shells [42]. The modelling of deformable structures allows the potential for modelling both granular materials and structures and their interaction within the same DEM framework.

Conclusions

This paper has presented the development, implementation and verification of a bonded particle model that enables the study of cemented particles and deformable structures using the Discrete Element Method in three dimensions. The key element of the developed model is the way in which inter-particle bonds are treated as Timoshenko beam elements. The model has been successfully

implemented in a commercial DEM code, allowing for the analysis of complex materials and structures.

The model has been shown to simulate the behavior of a concrete cylinder under uni-axial compression, and the predicted bulk response is in good agreement with the Eurocode prediction, showing significant potentials for further investigation. Although the model contains many input parameters, most can be kept constant whilst only a few need to be modified to produce a wide range of concrete behaviour. In practice this meant that, for a consistent particle packing and initial bond fabric, the bulk behaviour is controlled only by the bond Young's modulus and the mean bond tensile strength, some of the remaining parameters were linked to these variables. The main failure mode of the bonds is through tension, leading to a principle crack forming an inclined failure plane through the mid-height of the specimen. This failure mode is consistent with that seen in practice.

A unique feature of the new bond model is that it can be used to accurately represent the elastic behaviour of deformable structures, which is advantageous as both particles and deformable boundaries as well as their interaction can be simulated in the same DEM framework.

Acknowledgements

The authors would like to thank EPSRC and DEM Solutions Ltd for the funding and sponsorship. We are also grateful for the assistance and discussion with DEM Solutions.

References

1. Kuhl, E., D'Addetta, G.A., Herrmann, H.J., Ramm, E.: A comparison of discrete granular material models with continuous microplane formulations. Granular Matter. 2, 113–121 (2000).
2. Cundall, P.A.: A Computer model for simulating progressive large scale movement in blocky rock systems. Proceedings of the Symposium of the International Society of Rock Mechanics. , Nancy (1971).
3. Cundall, P.A., Strack, O.D.L.: A discrete numerical model for granular assemblies. Geotechnique. 29, 47–65 (1979).

4. Labra, C.: Advances in the development of the discrete element method for excavation processes, (2012).
5. Rojek, J., Labra, C., Su, O., Oñate, E.: Comparative study of different discrete element models and evaluation of equivalent micromechanical parameters. International Journal of Solids and Structures. 49, 1497–1517 (2012).
6. Ergenzinger, C., Seifried, R., Eberhard, P.: A discrete element model to describe failure of strong rock in uniaxial compression. Granular Matter. 13, 341–364 (2011).
7. Potyondy, D.O., Cundall, P.A.: A bonded-particle model for rock. International Journal of Rock Mechanics and Mining Sciences. 41, 1329–1364 (2004).
8. Cho, N., Martin, C.D., Sego, D.C.: A clumped particle model for rock. International Journal of Rock Mechanics and Mining Sciences. 44, 997–1010 (2007).
9. Su, O., Ali Akcin, N.: Numerical simulation of rock cutting using the discrete element method. International Journal of Rock Mechanics and Mining Sciences. 48, 434–442 (2011).
10. D'Addetta, G.A., Ramm, E.: A Microstructure-based Simulation Environment on the Basis of an Interface Enhanced Particle Model. Granular Matter. 8, 159–174 (2006).
11. Schneider, B., Bischoff, M., Ramm, E.: Modeling of material failure by the discrete element method. Proceedings in Applied Mathmatics and Mechanics. , Stuttgart (2010).
12. André, D., Iordanoff, I., Charles, J., Néauport, J.: Discrete element method to simulate continuous material by using the cohesive beam model. Computer Methods in Applied Mechanics and Engineering. 213-216, 113–125 (2012).
13. Carmona, H.A., Wittel, F.K., Kun, F., Herrmann, H.J.: Fragmentation processes in impact of spheres. Physical Review E. 77, 051302 (2008).
14. D'Addetta, G.A., Kun, F., Ramm, E.: On the application of a discrete model to the fracture process of cohesive granular materials. Granular Matter. 4, 77–90 (2002).
15. Schlangen, E., Garboczi, E.J.: Fracture simulations of concrete using lattice models:Computational aspects. Engineering Fracture Mechanics. 57, 2/3, 319-332 (1997)
16. Ostoja-Starewski, M.: Lattice models in micromechanics. Applied Mechanics Review. 50, 1, 35-59 (2002)
17. Lilliu, G., van Mier, J.G.M.: 3D lattice type fracture model for concrete. Engineering Fracture Mechanics. 70, 927-941 (2003)
18. Azevedo, N.M., Lemos, J.V., De Almeida, J.R.: Influence of aggregate deformation and contact behaviour on discrete particle modelling of fracture of concrete. Engineering Fracture Mechanics. 75, 1569–1586 (2008).
19. Camborde, F., Mariotti, C., Donze, F. V.: Numerical study of rock and concrete behaviour by discrete element modelling. Computers and Geotechnics. 27, 225–247 (2000).
20. Hentz, S., Donzé, F. V., Daudeville, L.: Discrete element modelling of concrete submitted to dynamic loading at high strain rates. Computers & Structures. 82, 2509–2524 (2004).
21. Qin, C., Zhang, C.: Numerical study of dynamic behavior of concrete by meso-scale particle element modeling. International Journal of Impact Engineering. 38, 1011–1021 (2011).

22. Magnier, S.A., Donze, F. V.: Numerical simulations of impacts using a discrete element method. 3, 257–276 (1998).
23. Sawamoto, Y., Tsubota, H., Kasai, Y., Koshika, N., Morikawa, H.: Analytical studies on local damage to reinforced concrete structures under impact loading by discrete element method. Nuclear Engineering and Design. 179, 157–177 (1998).
24. Przemieniecki, J.S.: Theory of matrix structural analysis. McGraw-Hill, New York (1968).
25. Wittel, F.K., Carmona, H.A., Kun, F., Herrmann, H.J.: Mechanics in impact fragmentation. International Journal of Fracture. 154, 105-117 (2008)
26. DEM Solutions: EDEM 2.1 User Guide, (2008).
27. Johnson, K.L.: Contact Mechanics. Cambridge University Press, Cambridge (1987).
28. Timoshenko, S.P.: X. On the transverse vibrations of bars of uniform cross-section. Philosophical Magazine Series 6. 43, 125–131 (1922).
29. Gere, J.M., Timoshenko, S.P.: Mechanics of materials. PWS-KENT (1990).
30. Johnstone, M.W.: Calibration of DEM models for granular materials using bulk physical tests, (2010).
31. Misra, A., Cheung, J.: Particle motion and energy distribution in tumbling ball mills. Powder Technology. 105, 222–227 (1999).
32. Tsuji, Y., Tanaka, T., Ishida, T.: Lagrangian numerical simulation of plug flow of cohesionless particles in a horizontal pipe. Powder Technology. 71, 239–250 (1992).
33. DEM.Solutions: EDEM 2.3, (2010).
34. Bažant, Z.P., Tabbara, M.R., Kazemi, M.T., Pyaudier-cabot, G.: Random particle model for fracture of aggregate or fiber composites. Journal of Engineering Mechanics. 116, (1991).
35. Hentz, S., Daudeville, L., Donzé, F.-V.: Identification and Validation of a Discrete Element Model for Concrete. Journal of Engineering Mechanics. 130, 709–719 (2004).
36. Tavarez, F.A., Plesha, M.E.: Discrete element method for modelling solid and particulate materials. International Journal for Numerical Methods in Engineering. 70, 379–404 (2007).
37. Ross, C.T.F., Case, J., Chilver, A.: Strength of Materials and Structures. Arnold, London (1999).
38. CIMNE: GiD, www.gidhome.com, (2012).
39. Labra, C., Escolano, E., Pasenau, M.: GiD features for discrete element simulations. 5th Conference on Advances and Applications of GiD. , Barcelona (2010).
40. O'Sullivan, C., Bray, J.D.: Selecting a suitable time step for discrete element simulations that use the central difference time integration scheme. Engineering Computations, 21(2/3/4), 278-303 (2004).
41. Cundall, P.A.: Distinct Element Models of Rock and Soil Structure. In: Brown, E.T. and Bray, J. (eds.) Analytical and Computational Methods in Engineering Rock Mechnics. pp. 129–163. Allen and Unwin, London (1987).
42. Brown, N.J.: Discrete Element Modelling of Cementitious Materials, (2013).

43. Dhir, R.K., Sangha, R.M.: Development and propagation of microcracks in plain concrete. Matériaux et Constructions. 7, 17–23 (1974).
44. Mehta, P.K., Monterio, P.J.M.: Concrete: Structure, Properties and Materials. Prentice Hall (1993).
45. Zhou, Y.-W., Wu, Y.-F.: General model for constitutive relationships of concrete and its composite structures. Composite Structures. 94, 580–592 (2012).
46. BS EN 1992-1-1: Eurocode 2: Design of concrete structures - Part 1-1: General rules and rules for buildings. (2004).
47. Neville, A.M., Brooks, J.J.: Concrete Technology. Longman Scientific & Technical, Harlow (1987).

Fig. 1 Projected view through the central axis of a bond connecting particles *A* and *B*

Fig. 2 Forces and moments acting at the ends of a bond in the local co-ordinate system

Fig. 3 A beam of length *L* made from connecting 5 particles with 4 bonds of length L_b

Fig. 4 Transverse deflection of the free particle over time

Fig. 5 Initial particle configuration

Fig. 6 Distribution of initial number of bonds per particle

Fig. 7 Stress-strain response and progression of broken bonds for the test case

Fig. 8 Bond failure mode against axial strain for the test case

Fig. 9 Slice through the centre of the specimen showing the main failure plane as broken bonds (black) and intact bonds (yellow) c post peak regime (at $\varepsilon = 0.0027$)

Fig. 10 DEM prediction versus Eurocode stress-strain curves for concrete strengths

Fig. 11 Progression of broken bonds in the DEM simulations for three concrete strengths

Table 1 Predicted central deflection compared with theoretical solution

Table 2 Input parameters for the Timoshenko Beam Bond Model

Table 3 Bond model parameters for the three cases

Table 4 Comparison of target and DEM predicted bulk properties

List of symbols

A	Area (m^2)
d	Translational displacement (m)
e	Coefficient of restitution
E	Young's modulus (Pa)

f_s	Form factor for shear
G	Shear modulus (Pa)
I	Second moment of area (m^4)
K	Stiffness ($N.m^{-1}$)
L	Length (m)
m	Mass (kg)
M	Moment (N.m)
N	Random number
P	Position
r	radius (m)
S	Mean bond strength (Pa)
t	Time (s)
u	Displacement vector (m)
W	Point load (N)
x, y, z	Local Cartesian coordinates (m, m, m)
X, Y, Z	Global Cartesian coordinates (m, m, m)
γ	Transformation matrix
δ	Mid-span deflection (m)
Δt	Time step (s)
ε	Strain
η	Contact radius multiplier
λ	Bond radius multiplier
μ	Coefficient of friction
ρ	Density ($kg.m^{-3}$)
ς	Coefficient of variation of strength
σ	Axial stress (MPa)
τ	Shear stress (Pa)
ν	Poisson's ratio

Indices (subscripts)

α, β	Ends of a single bond
A, B	Particle labels
b	Bond
c	Bulk

C	Compressive stress
$crit$	Critical
g	Geometry
min	Minimum
max	Maximum
ρ	Particle
r	Rolling friction
s	Static friction
S	Shear stress
T	Tensile stress
x, y, z	Local Cartesian coordinates
X, Y, Z	Global Cartesian coordinates

Table 1 Predicted central deflection compared with theoretical solution

Number of particles	DEM predicted central deflection (mm)	error %
3	28.7151	0.0061
5	28.7144	0.0086
17	28.7142	0.0093
31	28.7142	0.0093

Table 2 Input parameters for the Timoshenko Beam Bond Model

Parameter	Description	Value
ρ_p	Particle density (kg.m^{-3})	2700
E_p	Particle Young's modulus (GPa)	70
ν_p	Particle Poisson's ratio	0.25
μ_{sp}	particle-particle static friction	0.5
μ_{sg}	particle-geometry static friction	1
μ_{rp}	particle-particle rolling friction	0.5
μ_{rg}	particle-geometry rolling friction	0.0
e_{rp}	particle-particle restitution	0.5
e_{rg}	particle-geometry restitution	0.0001
E_b	Bond Young's modulus (GPa)	variable
ν_b	Bond Poisson's ratio	0.2
S_C	Mean bond compressive strength (MPa)	= 5×S_T
S_T	Mean bond tensile strength (MPa)	variable
S_S	Mean bond shear strength (MPa)	= S_T
ς_C	Coefficient of variation of compressive strength	0.0
ς_T	Coefficient of variation of tensile strength	0.8
ς_S	Coefficient of variation of shear strength	0.8

Table 3 Bond model parameters for the three cases

Property	Description	Case 1	Case 2	Case 3
f_c'	Target ultimate strength (MPa)	28	48	68
E_b	Bond Young's modulus (GPa)	28	40	50
S_T	Mean bond tensile strength (MPa)	60	105	150

Table 4 Comparison of target and DEM predicted bulk properties

	DEM prediction			% deviation from Eurocode		
	Case 1	Case 2	Case 3	Case 1	Case 2	Case 3
Ultimate strength f_c' (MPa)	28.4	48.5	67.8	1.6	1.1	-0.3
Bulk stiffness $E_{c\,(0.4)}$ (GPa)	18.5	26.9	33.1	-40.4	-27.6	-20.7
Strain at f_c' , ε_c	0.001969	0.002320	0.002586	0.1	-0.2	-0.1
Bulk Poisson's ratio ν_c	0.193	0.191	0.193	-	-	-

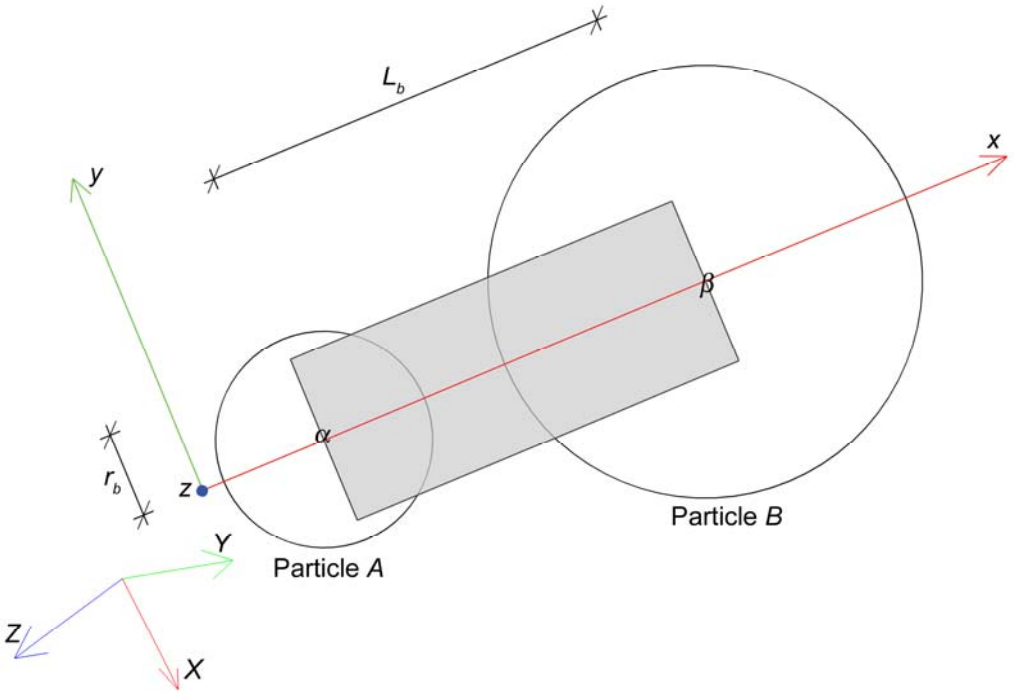

Fig. 1 Projected view through the central axis of a bond connecting particles A and B

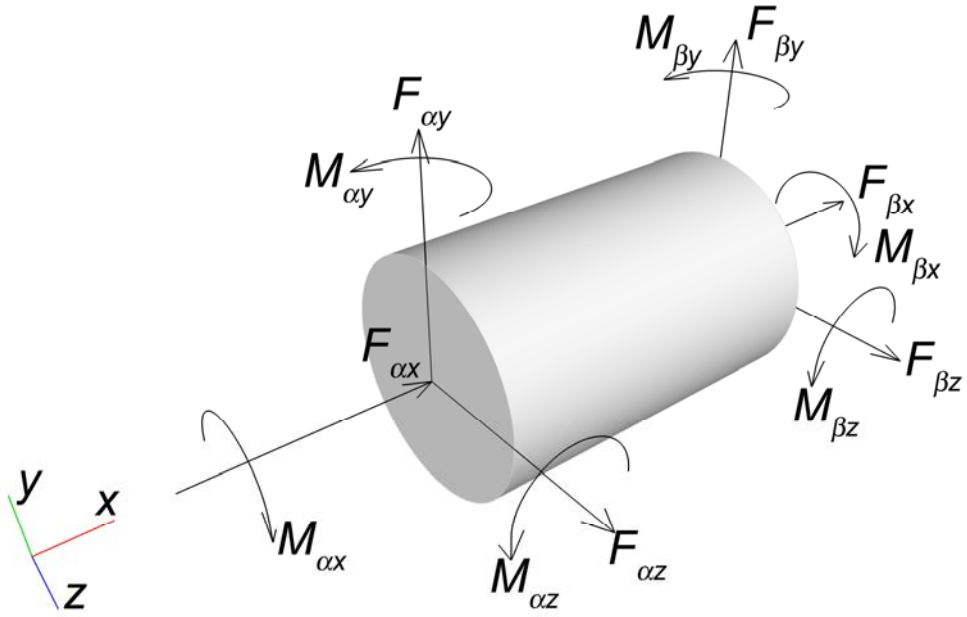

Fig. 2 Forces and moments acting at the ends of a bond in the local co-ordinate system

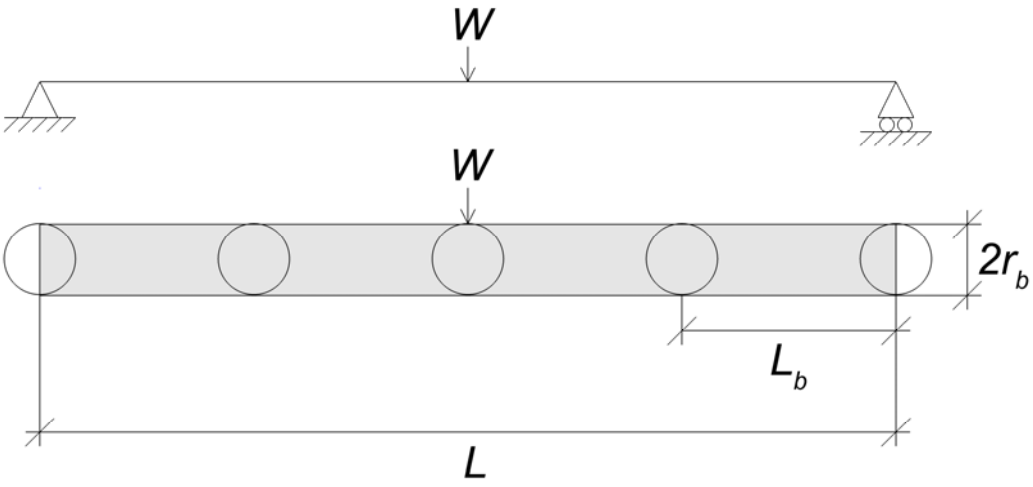

Fig. 3 Beam of length L made from connecting 5 particles with 4 bonds of length L_b

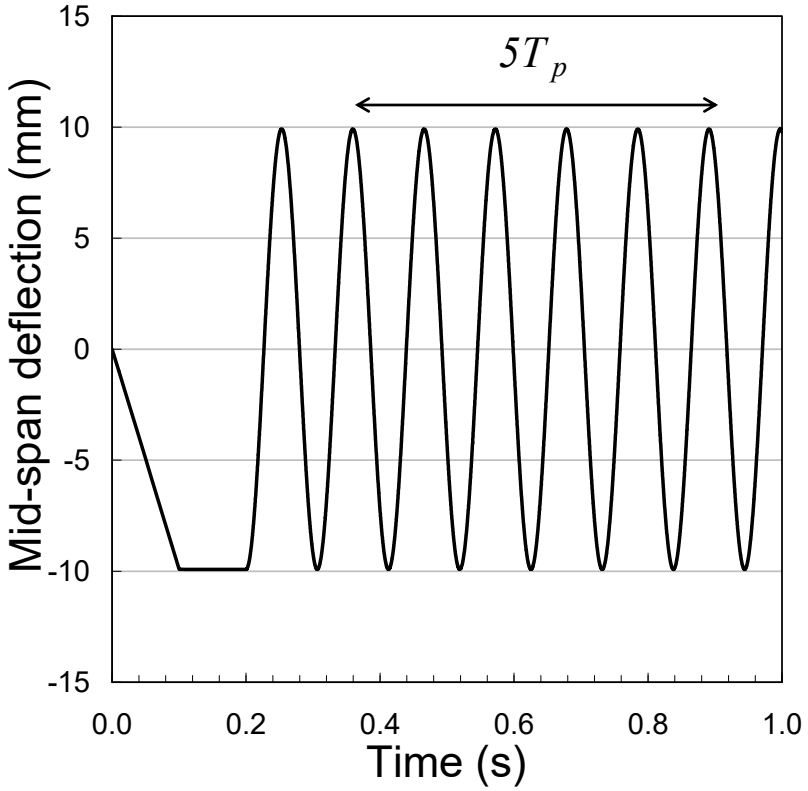

Fig. 4 Transverse deflection of the free particle over time

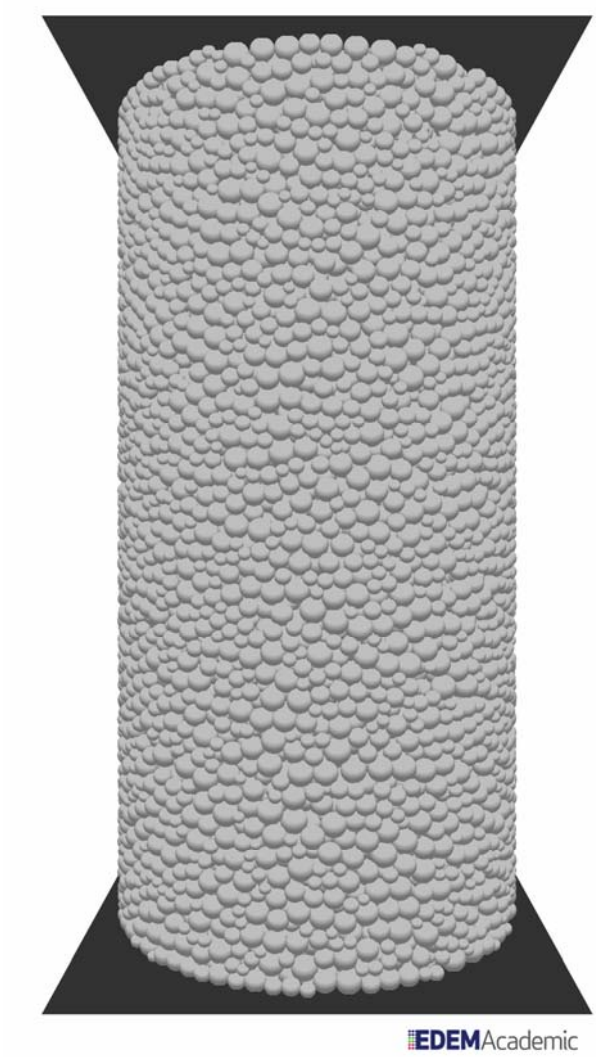

Fig. 5 Initial particle configuration

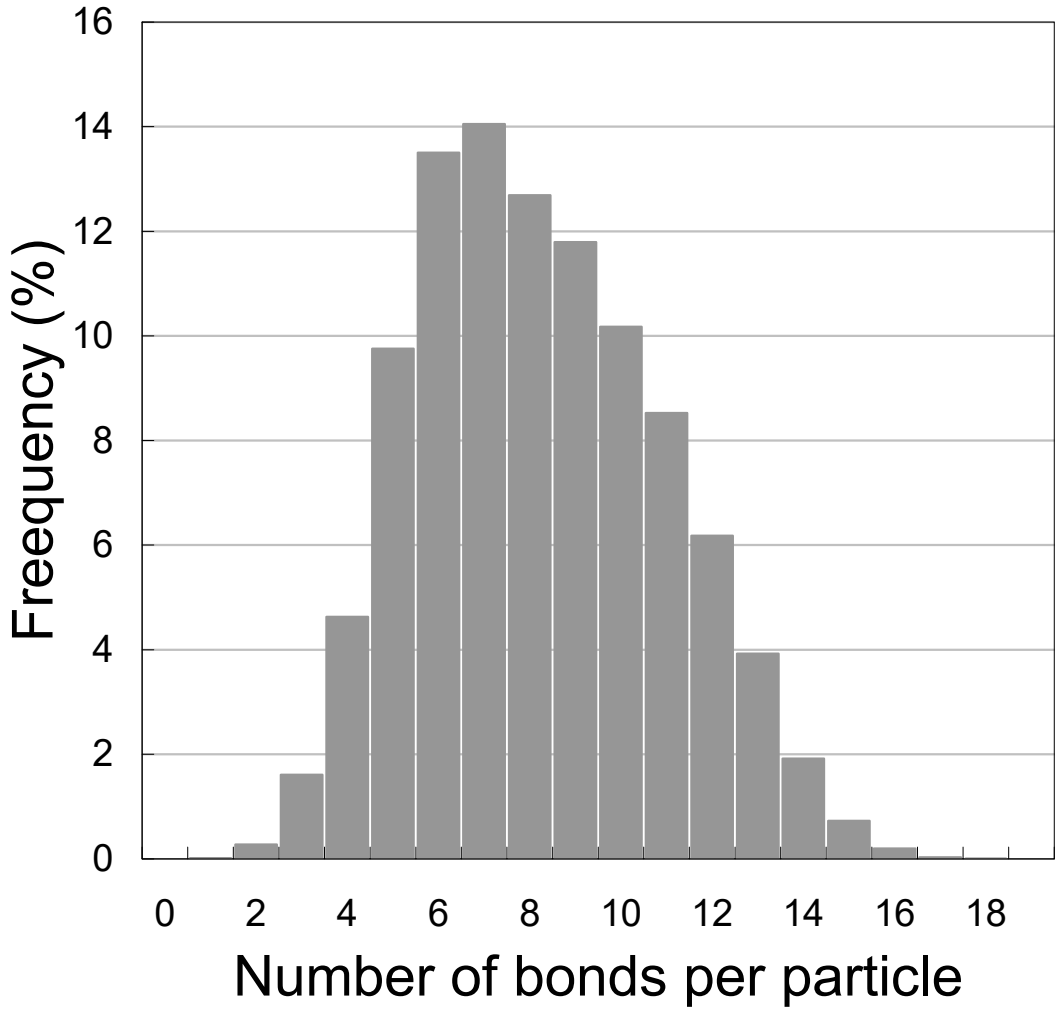

Fig. 6 Distribution of initial number of bonds per particle

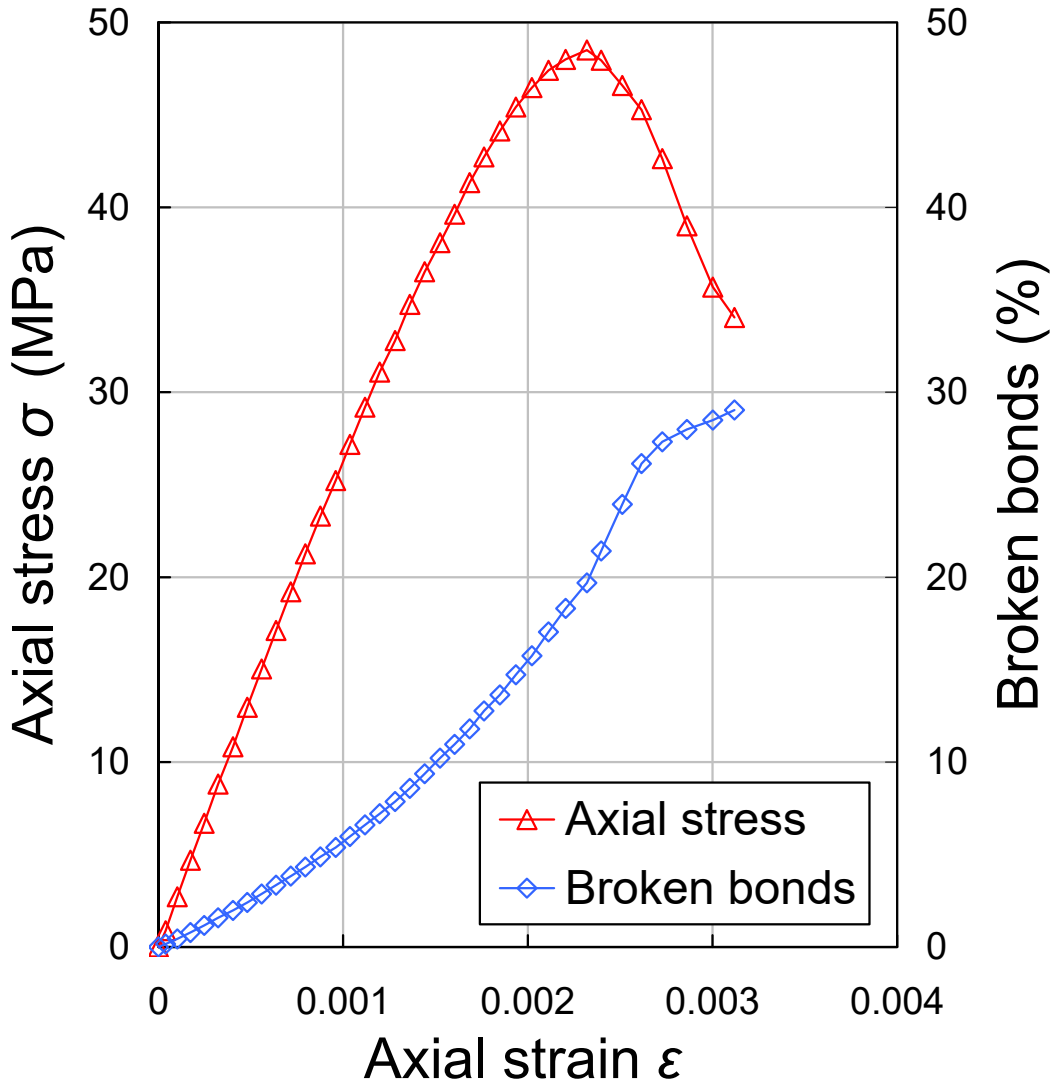

Fig.7 Stress-strain response and progression of broken bonds for the test case

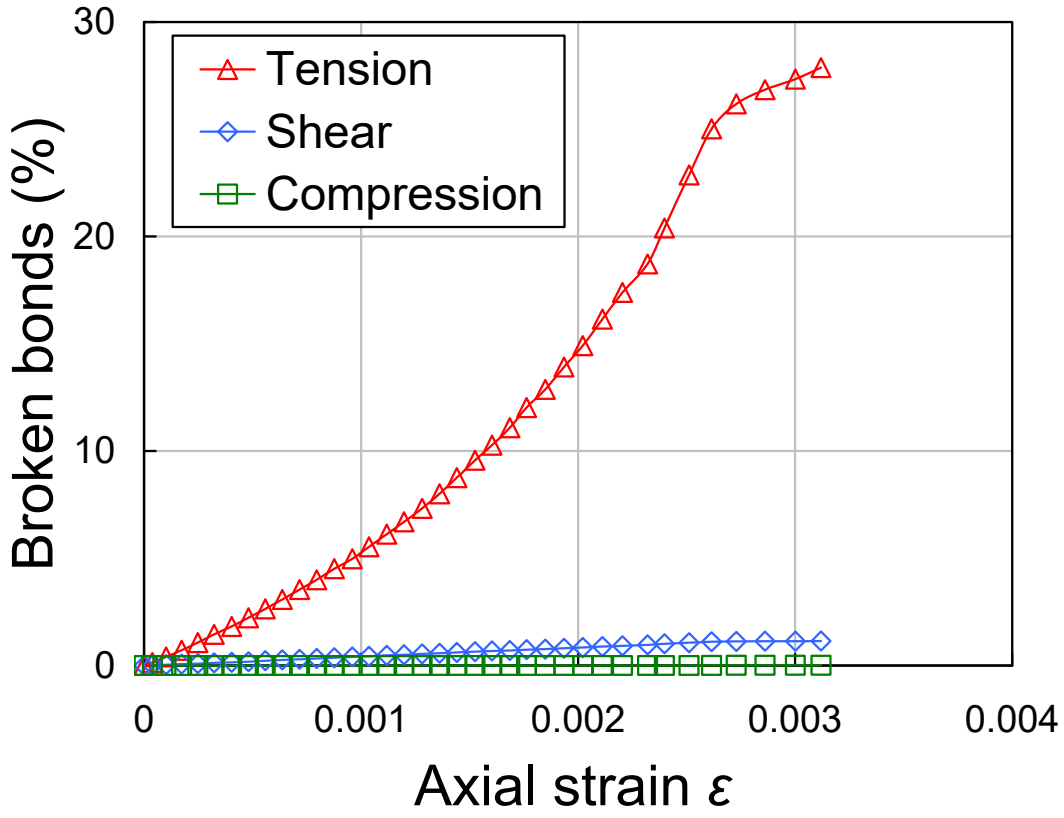

Fig. 8 Bond failure mode against axial strain for the test case

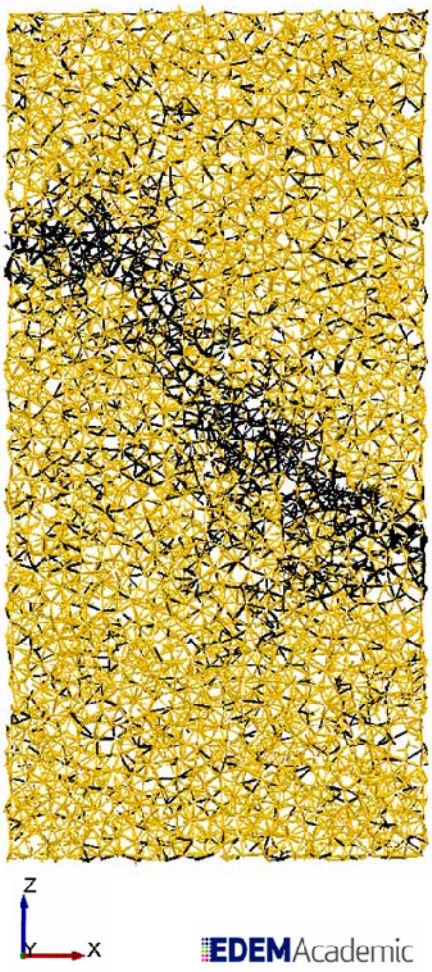

Fig. 9 Slice through the centre of the specimen showing the main failure plane as broken bonds (black) and intact bonds (yellow) at post peak regime (at $\varepsilon = 0.0027$)

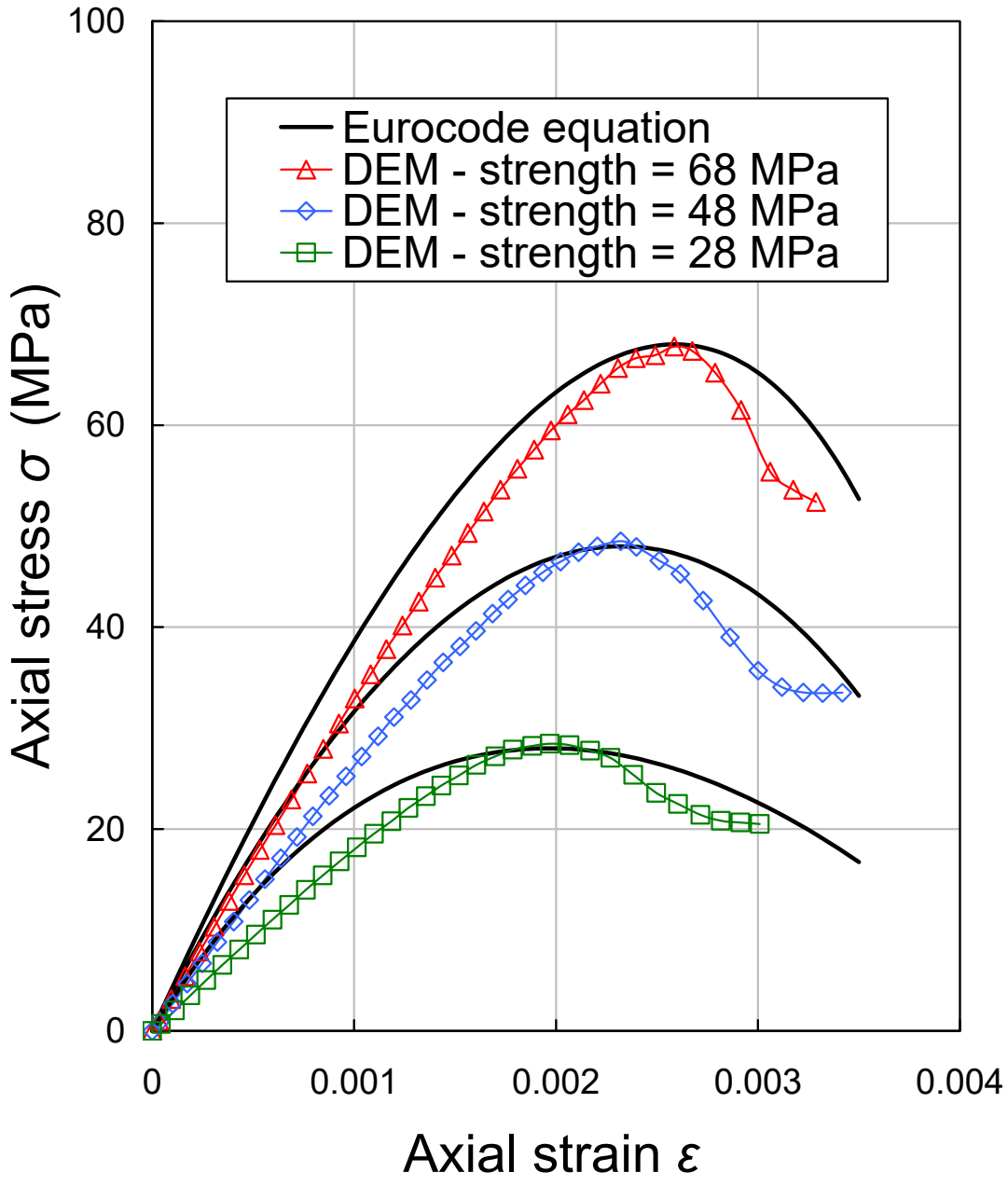

Fig. 10 DEM prediction versus Eurocode stress-strain curves for concrete strengths

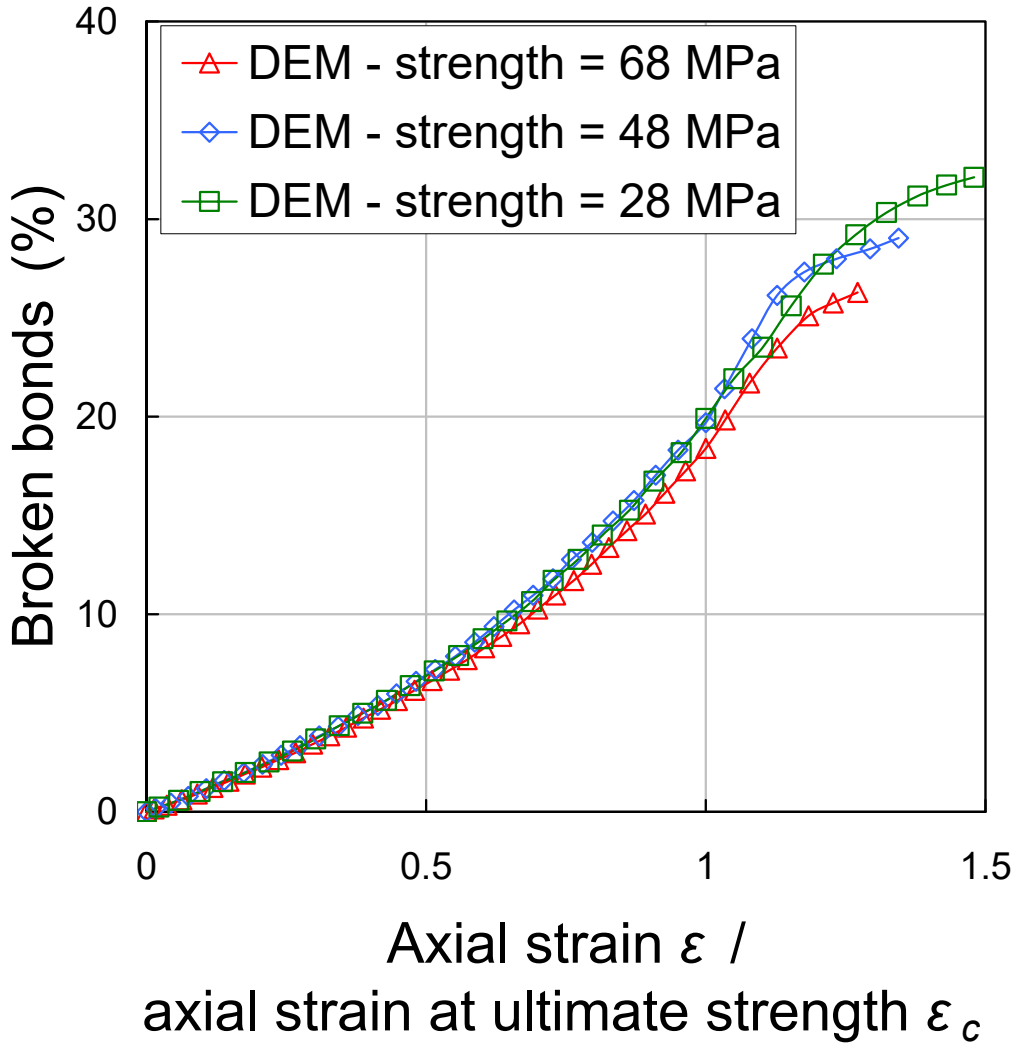

Fig. 11 Progression of broken bonds in the DEM simulations for three concrete strengths